Test results of Spacelab 2 Infrared Telescope focal plane

E. T. Young, G. H. Rieke, T. N. Gautier, W. F. Hoffmann, F. J. Low, W. Poteet

Steward Observatory, University of Arizona, Tucson, Arizona 85721

G. G. Fazio, D. Koch, W. A. Traub

Smithsonian Astrophysical Observatory, 60 Garden Street, Cambridge, Massachusetts 02138

E. W. Urban, L. Katz

Space Sciences Laboratory, Marshall Space Flight Center, Huntsville, Alabama 35812

Abstract

The small helium cooled infrared telescope for Spacelab 2 will permit sensitive mapping of extended, low-surface-brightness celestial sources as well as highly sensitive investigations of the shuttle contamination environment. The development of the focal plane array for this instrument is described. A number of the photoconductive detectors used in the focal plane were made at the University of Arizona, and we describe the fabrication procedure and some test results. A design for a thermally isolated, self-heated J-FET transimpedance amplifier is presented. This amplifier is Johnson noise limited for feedback resistances from less than 10^8 Ω to greater than 2×10^{10} Ω at T = 4.2K. Work on the focal plane array is now complete. Performance testing for qualification of the flight hardware is discussed, and results of this work are presented. All infrared data channels are measured to be background limited by the expected level of zodiacal emission.

I. Introduction

The small helium-cooled infrared telescope (IRT) for Spacelab 2 is a collaborative effort on the part of the University of Arizona (U of A), the Smithsonian Astrophysical Observatory (SAO), and the Marshall Space Flight Center (MSFC). This instrument will permit very high sensitivity observations of astronomical objects at a variety of infrared wavelengths and will make important engineering measurements that have bearing on future space infrared missions. The U of A is building the telescope, focal plane array, and focal plane electronics, MSFC is handling the cryogenic system, and SAO is responsible for overall project management, the data and control electronics, and data reduction.

The experiment has three primary goals. First, an infrared sky survey to high sensitivity and modest angular resolution is desired. Presently, virtually nothing is known about the diffuse, very-low surface brightness emission from the Galaxy and from extragalactic sources. Additionally, present measurements of the zodiacal background, especially at the longer wavelengths, are highly uncertain. Second, we plan to measure the contamination environment of the space shuttle. Particulate and gaseous contamination (especially H_2O and CO_2) from the shuttle may degrade future infrared observations, so we have designed the IRT to be especially sensitive to these backgrounds. To meet the first two experimental goals a highly sensitive, multi-band instrument is required, preferably background limited by the zodiacal emission. Finally, we will study the thermal performance of the telescope to better understand the properties of large, superfluid helium systems in the space environment.

Briefly the IRT consists (see Figure 1) of a cryostat (with sunshade) which contains a cooled 15 cm Herschelian telescope, a helium transfer assembly, a 250 l helium storage dewar, and the associated electronics. The cryostat scans in a 90° arc along an axis parallel to the long axis of the shuttle orbiter. Thus, overlapping strips of the sky are mapped as the orbiter circles the Earth. More detailed discussions of the telescope and mission are given by Gautier *et al.*[1] and Koch *et al.*[2] while the cryogenic system has been described by Urban *et al.*[3]

The present paper will describe the development of the ten-detector focal plane array (FPA) for this mission. A number of the infrared detectors were fabricated at the University of Arizona, and we will describe this work in the next section. The focal plane electronics are of unusual design and are considered in section IV. The final section presents some of the results of the testing program.

II. Infrared Detectors

For the low background conditions to be encountered in Spacelab, the most sensitive

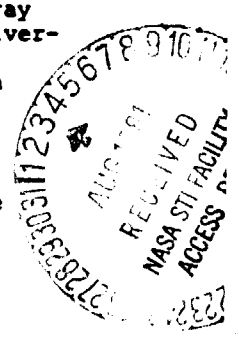

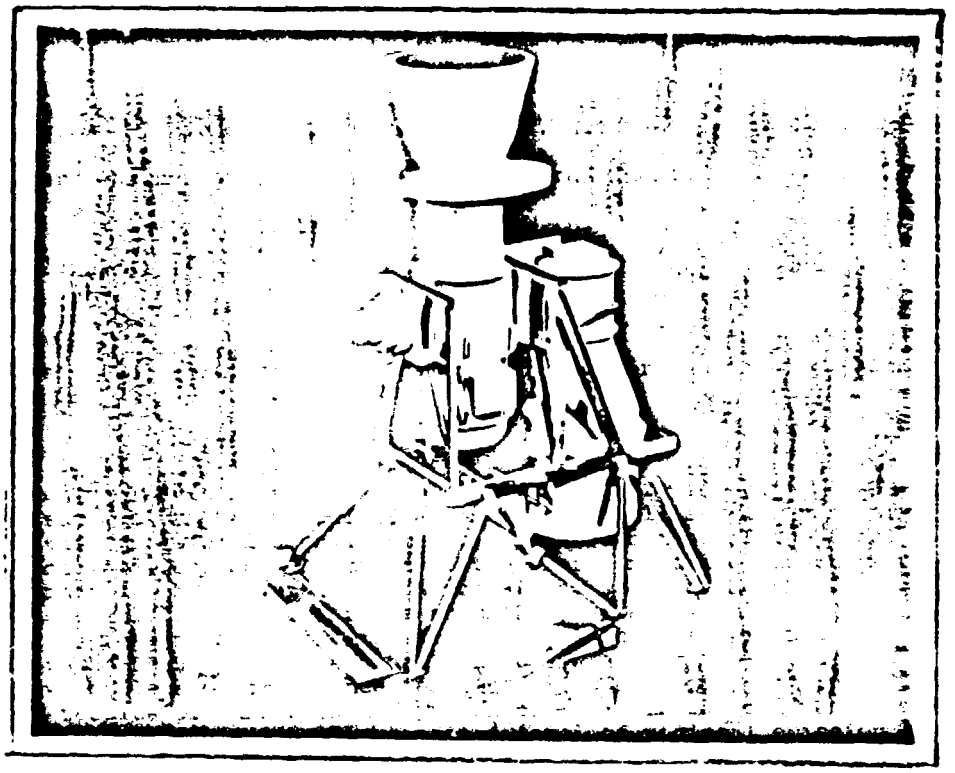

Figure 1. Scale model of Spacelab IRT showing cryostat, dewar, and mount. Actual experiment height is 340 cm.

infrared detectors are impurity doped silicon and germanium photoconductors. In support of the Spacelab IRT and the Infrared Astronomy Satellite (IRAS) projects, we have investigated the performance of a large number of detectors under low background conditions. Additionally, we have fabricated both silicon and germanium detectors successfully.

Photoconductors exhibit the highest quantum efficiency near the energy cutoff of the particular impurity level that is being excited. Thus, a multiband focal plane will likely use a number of detector materials. The Spacelab IRT will incorporate three detector types as indicated in Table 1. The gallium-doped silicon (Si:Ga) detectors were made by the Santa Barbara Research Center (SBRC). The antimony-doped silicon detectors were made at

Table 1. Spacelab Detectors

Band	λ(μm)	Detector Type	Source	Thickness (mm)
S	2-3	Si:Ga	SBRC	0.5
A	4.5-9.5	Si:Ga	SBRC	0.5
B	6-7	Si:Ga	SBRC	0.5
C	9-16	Si:Ga	SBRC	0.5
D1,D2,D3	18-30	Si:Sb	UA/RIC	1.0
E1,E2,E3	70-120	Ge:Ga	LBL	1.0

SBRC - Santa Barbara Research Center

UA/RIC - University of Arizona, material from Rockwell International Corp.

LBL - Lawrence Berkeley Laboratory, made by Dr. E. Haller

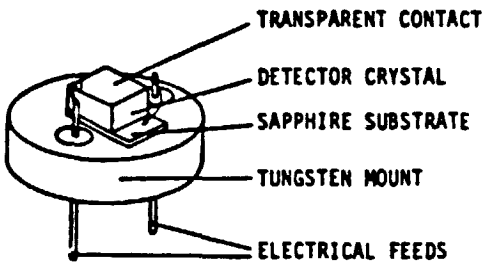

Figure 2. Detail of infrared detector.

the U of A from dies prepared by Dr. E. Haller of Lawrence Berkeley Laboratory. The preparation technique is similar to that for Ge:Sb described in Watson et al.[4]

Detector construction

Figure 2 shows the details of a Spacelab detector. The single crystal photoconductor is mounted on a sapphire substrate to provide electrical isolation from the tungsten mount. Tungsten is used throughout the Spacelab focal plane to provide a degree of shielding from cosmic radiation. The quality of the contacts on the semiconductor material is critical to the performance of the detector. Although this technology has been something of an art in the past, consistently successful contacts are now possible with ion implantation. The ion implanted front and back surfaces are then metalized with vacuum evaporated (or sputtered) titanium-gold for connection to leads.

We have obtained several slices of antimony doped silicon (Si:Sb) from the IRAS project for detector research. This material was manufactured by the Rockwell International Corporation. The slices were ion implanted at the Microelectronics Laboratory of the University of Arizona with 100 KeV phosphorous ions at a concentration of 10^{14} cm^{-2}. Subsequent steps are:

1. Thermal annealing of implantation layer
2. Cleaning with $H_2SO_4 + H_2O_2$ solution
3. HF etch
4. Titanium + gold metalization
5. Dicing into detectors
6. Polish etch of detector sides
7. Mounting on substrates

Testing of these detectors has shown them to be very high quantum efficiency devices, and four of them are used in the Spacelab FPA.

III. Detector testing

Test conditions

The detector test unit is designed to accurately simulate conditions expected in the Spacelab mission, in particular the low background conditions. The apparatus consists of a side-looking Infrared Laboratories dewar and an externally chopped blackbody. We have employed a combination of neutral density attenuators and very restricted fields of view to limit background irradiation to zodiacal levels. For example, the Si:Sb detectors are tested at backgrounds of $\sim 1 \times 10^8$ photons s^{-1}. The test unit has been described in greater detail by Young and Low[5] with the only enhancement being the replacement of the MOSFET electronics with a J-FET equivalent. The use of J-FET's in photoconductor circuits is discussed in Section V.

We have measured responsivity and noise as functions of background power, bias voltage, and frequency. Additional characteristics that have been investigated include the temperature dependence of the detectivity, the spontaneous spiking behavior, and anomalous time

Table 2. Detector Test Results

Detector	Type	Bias(V)	Background (W)	Responsivity (A/W)	NEP (W $Hz^{-\frac{1}{2}}$)	η (%)
SBRC 726	Si:Ga	12	3.3×10^{-14}	2.0	9.3×10^{-17}	25
SBRC 727	Si:Ga	12	3.3×10^{-14}	2.1	8.2×10^{-17}	32
UA 113	Si:Sb	4	6.4×10^{-12}	0.98	5.1×10^{-16}	83
UA 117	Si:Sb	4	6.4×10^{-12}	0.80	5.0×10^{-16}	85
LBL 2	Ge:Ga	0.15	3.2×10^{-13}	3.8	4.2×10^{-16}	3
LBL 4	Ge:Ga	0.15	3.2×10^{-13}	3.8	3.3×10^{-16}	5

constants in the detectors. In general, we have found that problems with spontaneous spiking and anomalous time constants are minimized at reduced bias.

Results

Table 2 presents some representative results of the detector testing at the U of A. The backgrounds are typical for Spacelab conditions and the bias voltages are chosen as a best compromise between responsivity and anomalous behavior.

In all cases the detector active area is 2.5 mm x 2.5 mm. For the Ge:Ga testing, the detectors were placed in an integrating cavity with a 2 mm entrance aperture. The detective quantum efficiency η is defined by:

$$\eta = \left(\frac{NEP_{BLIP}}{NEP} \right)^2$$

IV. Spacelab focal plane optics

The Spacelab IRT focal plane consists of ten channels. These ten channels are distributed among four independent modules. The modular approach was chosen to allow the greatest flexibility during construction and testing. Each module, with two or three detectors, has its own electronics module and interface connector so that the units can be qualified for the mission individually. Figure 3 is a photograph of the completed FPA mounted on the fiberglass support fixture.

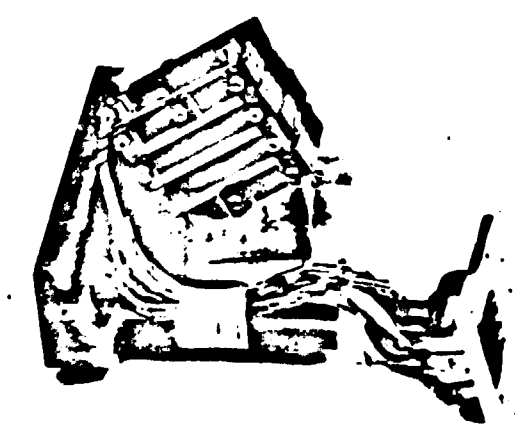

Figure 3. Completed focal plane array attached to fiberglass mount.

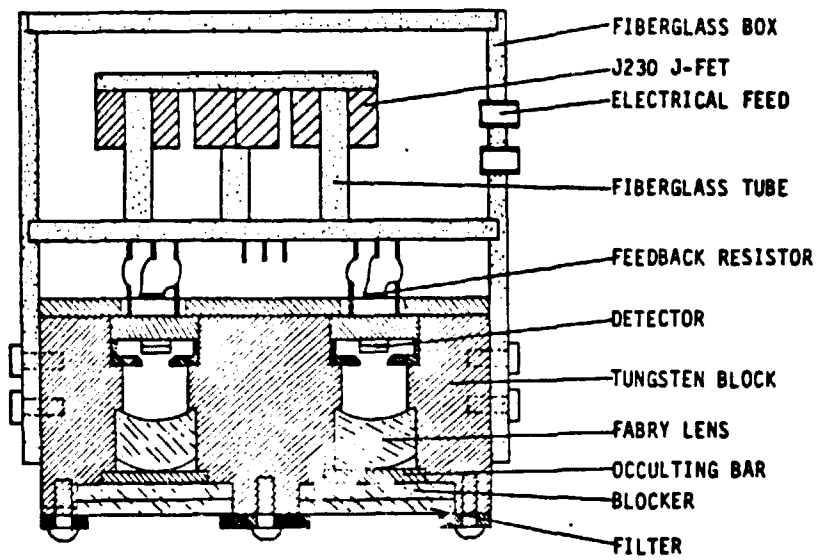

Figure 4. Cross sectional view of channel S-A focal plane module.

Figure 4 is a cross-sectional view of a representative module, the S-A segment. Bandpasses are determined with multilayer interference filters, and additional blocking is accomplished with crystaline elements. The Fabry optics are germanium meniscus lenses except for the D-channels which are silicon lenses. Each detector has a nominal field of view of 1° x 0.6° on the sky, however, a 12 arc minute wide strip is blocked by an occulting bar. This bar, which is perpendicular to the scan direction, modulates a point source into two pulses during a scan. This technique allows point sources to be located to within several arc minutes in the scan direction.

The Ge:Ga detectors used in the E channels have fairly low absorption coefficients, and hence show improved responsivities when placed in integrating cavities. A Spacelab far infrared channel uses a hemispherical cavity around the detector that is fed by a horn of 2.5 mm diameter entrance aperture and 1.57 mm diameter exit aperture. We find typically a factor of 2 or 3 improvement in responsivity over a bare Ge:Ga detector.

V. Focal plane electronics

The transimpedance amplifier (TIA) (see Ref. 6, 7, and 8) used in the Spacelab IRT is shown schematically in Figure 5. This circuit configuration was chosen primarily because of the extended high frequency response. The effective input capacitance of the input stage (the usual frequency limitation in a source follower) is reduced roughly by a factor of the open loop gain of the operational amplifier. Additionally, the bias voltage on the detector remains constant under varying signals, and the output is directly proportional to the detector photocurrent.

Early versions of the TIA used MOSFET's operating at liquid helium temperatures. Because of high MOSFET voltage noise, however, (~ 300 nV $Hz^{-\frac{1}{2}}$ @ 5 Hz in the best G118 devices) the systems were usually limited by amplifier noise rather than the Johnson noise of the feedback resistor. A second problem associated with operating MOSFET's below 15 K is a lack of D. C. stability in the source voltage.

The present Spacelab FPA uses Siliconix J230 J-FETs as a first stage to the TIA. These devices combine low noise (5 nV $Hz^{-\frac{1}{2}}$ @ 10 Hz) with low input capacitance (2 pF). The primary complication stems from the dual requirements of close proximity to the detectors but operation at temperatures above 50 K. Figure 4 shows the thermal isolation procedure used.

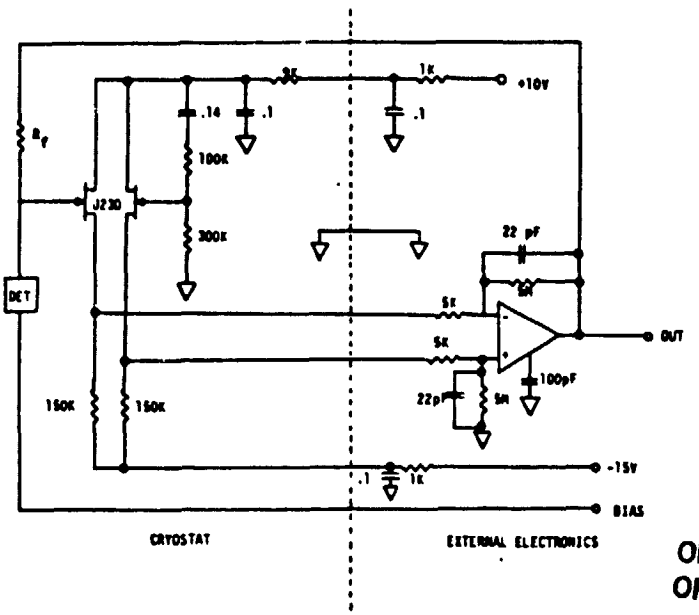

Figure 5. Schematic of transimpedance amplifier circuit used in IRT.

A substrate carrying three matched pairs of JFETs is supported on thinwall (2.2 mm diameter, 0.15 mm wall thickness) fiberglass tubes. Electrical connections are made with 3-mil constantan wire. The internal power dissipation of 1 mW for each J-FET is sufficient to heat them to ~ 80 K. To prevent photons from the heated JFETs from interfering with the detectors, the electronics are surrounded by a copper-clad fiberglass enclosure.

We have operated these JFET amplifiers with feedback resistances ranging from 10^9 Ω to 2×10^{10} Ω and find the noise to be Johnson limited by the feedback resistor. The noise spectra are flat from low frequencies to a roll off at $f \approx 1/2\pi R_f C_f$ where R_f is the feedback resistance and C_f the shunt capacitance of the feedback resistor. C_f is typically 0.05 pF.

A much more complete discussion of JFET use with infrared detectors is given by Low.[8]

VI. System performances

Test conditions

Low background tests of the focal plane modules were performed in a large dewar that contained a low temperature blackbody source with shutter and a variable background source. Special precautions were taken to eliminate any photon leaks in the test chamber so that Q_{ZILCH} conditions (< 10^6 photons s^{-1}) were realized even in the far infrared bands. With the variable background source, in-band irradiances of greater than 10^9 photons s^{-1} were achieved.

A typical test sequence consisted of measurements of signal and noise for the channels as functions of background and detector bias voltage. Figure 6 is a representative plot of noise voltage as a function of background for channel E1. Note that at very low background levels the amplifier is Johnson noise limited by the feedback resistor. Second, the background noise increases as the square root of the background power, as expected for photon statistics. Finally, the channel will be zodiacal background limited if the current models for this background are correct. Here we use the revised IRAS model:

$$F_\lambda = \frac{2.5 \times 10^{-6}}{\lambda(\mu m)} \quad B_\lambda (230) \qquad (W\ cm^{-2} sr^{-1} \mu m^{-1})$$

Table 3 summarizes the low background performance of the Spacelab 2 IRT. It should be emphasized that the sensitivities quoted are measured for the actual flight hardware. All channels except S, the aspect sensor, meet the sensitivity goal of being limited by the

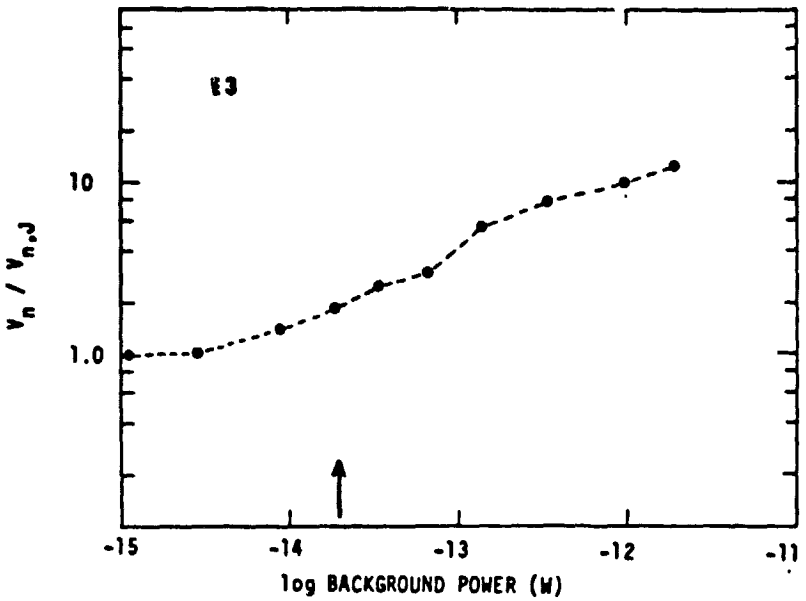

Figure 6. Plot of noise vs. background for E1 channel. Arrow indicates predicted zodiacal background level for this band.

Table 3. Characteristics of Spacelab IR Telescope Detector Channels

Band	Δ (μ)	V_B (volts)	S (A/W)	η (%)	ε (%)	R_f (Ω)	Q (W)	NEP_Q ($W/Hz^{\frac{1}{2}}$)	NEP_D ($W/Hz^{\frac{1}{2}}$)	NEFD ($W\ cm^{-2}\mu m^{-1}Hz^{-\frac{1}{2}}$)
S	2.0-3.0	22	0.03	~ 6	70	1.7×10^{10}	1.2×10^{-13}	8×10^{-16}	3×10^{-15}	2.42×10^{-17}
A	4.5-9.5	14	0.45	40	50	3×10^{9}	2.4×10^{-12}	8×10^{-16}	5×10^{-16}	1.8×10^{-18}
B	6.1-7.1	14	0.45	40	70	1.7×10^{10}	4.4×10^{-13}	3.6×10^{-16}	2×10^{-16}	2.9×10^{-18}
C	8.5-14	19	0.85	45	70	9×10^{8}	4.7×10^{-12}	9×10^{-16}	5×10^{-16}	1.3×10^{-18}
D	18-29.5	4	1.4	60	40	3×10^{9}	1.7×10^{-12}	3.4×10^{-16}	2×10^{-16}	4.0×10^{-19}
E	70-120	0.15	3	3	50	3×10^{9}	3.7×10^{-14}	1.5×10^{-16}	7×10^{-17}	3.4×10^{-20}

Definitions:

$\Delta\lambda$: wavelength range between half power points of effective filter transmission curve, including spectral characteristics of detectors, blockers, and optics

V_B: detector bias voltage

S : detector responsivity in the spectral band

η : detector quantum efficiency in the spectral band

ε : optical efficiency

R_f: feed back resistor

Q : background flux (zodiacal) incident on the detector

NEP_Q: background limited NEP

NEP_D: zero-background NEP

NEFD: noise equivalent spectral flux density, background limited

zodiacal background. The S channel will be able to detect a star of K-magnitude 3 at a signal to noise ratio of 20 in 16 ms, meeting the design requirements. As an example of what these sensitivity levels translate to during the mission, consider the detectability of H_2O contamination from the shuttle. Using the calculated H_2O emission spectrum of Simpson and Witteborn,[9] the Spacelab IRT B channel will be able to sense a column density of less than 2×10^9 molecules/cm^2. This level is much lower than predicted for the actual shuttle environment.

We have performed additional testing of other system characteristics. In particular the frequency response of the detector and electronics is important in discriminating between cosmic ray hits and genuine infrared sources. All the detector channels have useful response beyond 1 KHz, so the spikes (which last < 1 ms) will be easily distinguishable from the true sources (which last > 16 ms).

VII. Current status and continuing work

Work on the focal plane is now complete, and the unit has been qualified for the Spacelab 2 mission. Integration with the other components in the system is in progress leading to scheduled launch in November 1983.

We are extending our photoconductor work to significantly lower backgrounds. Initially, Si:Sb are being investigated under these conditions. For these experiments the feedback resistor is increased 20-fold to 2×10^{11} Ω. The J-FET transimpedance amplifier functions satisfactorily at these impedances albeit with a high frequency rolloff at ~ 30 Hz. A limiting NEP of 5×10^{-18} W Hz$^{-\frac{1}{2}}$ has been achieved in the 18-30 μm band with 8V bias. The main difficulty with operation in this regime is the strong tendency of Si:Sb detectors to spike at higher biases.

Acknowledgements

We wish to thank Dr. J. Fordemwalt of the U of A Microelectronics Laboratory and especially Dr. E. Haller of Lawrence Berkeley Laboratory for invaluable assistance in detector fabrication. This work is supported by the National Aeronautics and Space Administration.

References

1. Gautier, T. N., III, Rieke, G. H., Low, F. J., and Hoffmann, W. F. 1979, Proc. SPIE, 172, 264.
2. Koch, D., Fazio, G. G., Traub, W. A., Rieke, G. H., Gautier, T. N., Hoffmann, W. F., Low, F. J., Poteet, W., Young, E. T., Urban, E. W. and Katz, L. 1981, Proc. SPIE, 265, 257.
3. Urban, E. W., Katz, L., Hendricks, J. B., and Karr, G. R. 1979, Proc. SPIE, 183, 40.
4. Watson, D. M., Storey, J. W. V., Townes, C. H., and Haller, E. E. 1980, Astrophys. J. (Letters), 241, L43.
5. Young, E. T. and Low, F. J. 1979, Proc. SPIE, 172, 184.
6. Wyatt, C. L., Baker, D. J., and Frodsham, D. G. 1974, I. R. Phys., 14, 165.
7. Luinge, W., Wildeman, K. J., and van Duinen, R. J. 1980, I. R. Phys., 20, 39.
8. Low, F. J. 1981, Proc. SPIE, 280 (this volume).
9. Simpson, J. P. and Witteborn, F. C. 1977, Appl. Opt., 16, 2051.